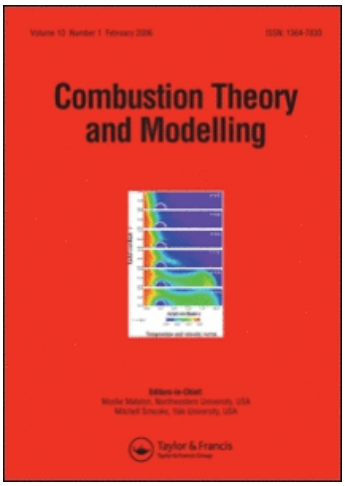

Combustion Theory and Modelling
Publication details, including instructions for authors and subscription information:
http://www.informaworld.com/smpp/title~content=t713665226

The cellular structure of a two-dimensional $H_2/O_2/Ar$ detonation wave

X. Y. Hu [a]; B. C. Khoo [a]; D. L. Zhang [b]; Z. L. Jiang [b]
[a] Singapore-MIT Alliance, National University of Singapore, Singapore [b] Laboratory of High Temperature Gas Dynamics, Institute of Mechanics, Beijing, People's Republic of China

Online Publication Date: 02 April 2004

To cite this Article Hu, X. Y., Khoo, B. C., Zhang, D. L. and Jiang, Z. L.(2004)'The cellular structure of a two-dimensional $H_2/O_2/Ar$ detonation wave',Combustion Theory and Modelling,8:2,339 — 359

To link to this Article: DOI: 10.1088/1364-7830/8/2/008

URL: http://dx.doi.org/10.1088/1364-7830/8/2/008

INSTITUTE OF PHYSICS PUBLISHING COMBUSTION THEORY AND MODELLING

Combust. Theory Modelling **8** (2004) 339–359 PII: S1364-7830(04)64376-2

The cellular structure of a two-dimensional $H_2/O_2/Ar$ detonation wave

X Y Hu[1], B C Khoo[1], D L Zhang[2] and Z L Jiang[2]

[1] Singapore-MIT Alliance, National University of Singapore, 4 Engineering Drive 3, 117576, Singapore
[2] Laboratory of High Temperature Gas Dynamics, Institute of Mechanics, Beijing, 100080, People's Republic of China

Received 4 June 2003, in final form 15 March 2004
Published 2 April 2004
Online at stacks.iop.org/CTM/8/339
DOI: 10.1088/1364-7830/8/2/008

Abstract

In this paper, the cellular structure of a two-dimensional detonation wave in a low pressure $H_2/O_2/Ar$ mixture calculated with a detailed chemical reaction model, high order scheme and high resolution grids is investigated. The regular cellular structure is produced about 1 ms after introducing perturbations in the reaction zone of a steady one-dimensional detonation wave. It is found from the present resolution study that the discrepancies concerning the structure type arising from the coarser grid employed can be resolved using a sufficiently fine grid size of 0.05 mm and below and shows a double-Mach-like strong-type configuration. During the structure evolution process, the structure configuration does not change much in the periods before and after the triple point collision. Through the triple point collision, three regular collision processes are observed and are followed by a quick change to the double-Mach-like configuration. The simulated structure tracks show that there are three different tracks associated with different triple points or the kink on the transverse wave. Comparisons with previous work and experiments indicate the presence of a strong structure for an ordinary detonation.

1. Introduction

It is well known that a gaseous detonation wave has a cellular structure. The tracks of this structure, recorded on smoke foils, have been observed in experiments, and the regions enclosed by these tracks are called detonation cells. Even though the structure has complex three-dimensional characteristics, somehow it still leaves very regular cell tracks, especially for rectangular or planar mode detonation of a low pressure $H_2/O_2/Ar$ mixture in rectangular channels and hence can be possibly idealized to two-dimensions approximately. The structure usually involves a triple-wave/Mach configuration, with the combination of an incident shock wave (I), Mach stem (M) and transverse wave (T). Two types of structure, i.e. a weak structure and a strong structure, are observed in experiments. The weak structure is characterized by a

single-Mach configuration, with the associated transverse wave being merely a shock wave, while the strong structure is characterized by a multi-Mach configuration with a much stronger transverse wave, leading to strong ignition. Gaseous detonations are also classified into two types, an ordinary detonation and a marginal detonation. Experiments show that an ordinary detonation has an average detonation velocity close to D_{CJ}, while a marginal one only has one of about $0.85D_{\mathrm{CJ}}$. It is widely accepted that in a marginal detonation the cellular structure is of the strong type and can be observed directly in experiments. As a much smaller detonation cell size than that found in a marginal detonation and the associated structure cannot be resolved easily and directly through experiments, it is still quite an open issue whether an ordinary detonation possesses a strong structure. Some indirect evidence that has been presented has also led to disagreements: for example, light was found in experiments of ordinary detonations, which suggests a strong structure with ignition of transverse waves (Voitsekhovskii *et al* 1963), but single-track smoke foil records of ordinary detonations have indicated a weak structure, as characterized by a single-Mach configuration (Strehlow 1969).

From the late 1970s, numerical simulation has been employed and increasingly so to study the cellular structure to reveal details that cannot be determined easily in experiments. In the early works, simple one- or two-step chemical reaction models were used, and the calculated results showed a typical triple-wave configuration (Taki and Fujiwara 1978). Finer spatial resolution numerical simulations with simple reaction models have also been used to study the detailed structure (Quirk 1993, Lefebvre and Oran 1995, Gamezo *et al* 1999). In addition, the multi-step, detailed reaction model has been employed with some success. With this model, Oran *et al* (1991, 1998) calculated the triple-wave configuration for a low pressure $H_2/O_2/Ar$ mixture. It is found that after the triple point collision, the structure evolves from a single-Mach configuration to double-Mach and more complex configurations. However, the coarser resolution employed may have led to some disagreement, as shown by Sharpe (2001). Sharpe used a very high spatial resolution numerical simulation for the same mixture but with simple reaction models. The results showed that the structure has a double-Mach-like configuration of the strong type and there is no further change before and after the triple point collision. Sharpe also commented that sufficient spatial resolution is absolutely necessary to resolve the structure well. However, the simple chemical reaction model utilized may have led to the loss of some fine features usually characterized by the complex chain-branching reaction process. Therefore, a sufficiently high resolution and complex detailed chemical reaction model are both needed to clarify/resolve the structure configuration and its evolution behaviour.

In this paper, the cellular structure is investigated through two-dimensional numerical simulations with a high resolution and detailed reaction model. The regular structure formation process is presented first, and the resolution study is performed. This is followed by a study of the structure configuration in great detail with the necessary high resolution. Next, the evolution of the structure before, through and after the triple collision is investigated. The numerics is compared with experiments and previous calculations, and a discussion on its relations to an ordinary detonation is also presented.

2. Physical and numerical models

Assuming no viscosity, radiation and other dissipation effects, the governing equations for the idealized two-dimensional gaseous detonation with N species and a multi-step chemical reaction model are given as

$$\frac{\partial \boldsymbol{U}}{\partial t} + \frac{\partial \boldsymbol{F}}{\partial x} + \frac{\partial \boldsymbol{G}}{\partial y} = \boldsymbol{S}, \tag{1}$$

where

$$\boldsymbol{U} = \begin{pmatrix} \rho \\ \rho u \\ \rho v \\ E \\ \rho_1 \\ \vdots \\ \rho_{N-1} \end{pmatrix}, \quad \boldsymbol{F} = \begin{pmatrix} \rho u \\ \rho u^2 + p \\ \rho u v \\ (E+p)u \\ \rho_1 u \\ \vdots \\ \rho_{N-1} u \end{pmatrix}, \quad \boldsymbol{G} = \begin{pmatrix} \rho v \\ \rho u v \\ \rho v^2 + p \\ (E+p)v \\ \rho_1 v \\ \vdots \\ \rho_{N-1} v \end{pmatrix}, \quad \boldsymbol{S} = \begin{pmatrix} 0 \\ 0 \\ 0 \\ 0 \\ \dot{\omega}_1 \\ \vdots \\ \dot{\omega}_{N-1} \end{pmatrix}.$$

This set of equations describes the conservation of density (ρ), momentum $\rho \boldsymbol{v} \equiv (\rho u, \rho v)$, total energy density ($E$) and density of species $\{\rho_i\}$, where $i = 1, N$. To close this set of equations, the total energy density is defined as

$$E = \rho h - p + \frac{\rho(u^2 + v^2)}{2}, \tag{2}$$

where the enthalpy (h) and pressure (p) are calculated using the thermochemical relation $h = h(\rho_i, T)$ (Stull 1971) and the equation of states, $p = p(\rho_i, T)$, for a thermally perfect gas, respectively. These equations have been non-dimensionalized using the upstream density (ρ^*_∞), sound speed (a^*_∞), temperature (T^*_∞) and the calculated reaction zone length (l^*) of one-dimensional steady detonation.

In this paper, a nine-species, 19 elementary reactions model is used for hydrogen–oxygen combustion (Wilson and MacCormack 1990). The reacting species are H_2, O_2, H, O, OH, H_2O_2, HO_2 and H_2O, and dilute argon is added to the gas mixture. The finite production rate of each chemical species, $\dot{\omega}$, is obtained by combining the elementary chemical reactions in the kinetic model so that

$$\dot{\omega}_i = W_i \sum_{k=1}^{K} (\nu''_{ik} - \nu'_{ik}) \left(K_{f,k} \prod_{i=1}^{N} (C_{\chi i})^{\nu'_{ik}} - K_{b,k} \prod_{i=1}^{N} (C_{\chi i})^{\nu''_{ik}} \right), \tag{3}$$

where $C_{\chi i} = \rho_i / W_i$ is the mole concentration of species i, and $K_{f,k}$ and $K_{b,k}$ are the forward and backward reaction rate constants, which are controlled by Arrhenius law and chemical equilibrium conditions.

In this work, a modified finite difference scheme employed based on the third-order ENO-LLF scheme, which is capable of resolving different discontinuities accurately and has a small numerical dissipation (Shu and Osher 1989), is first used. For low resolution (grid sizes of 0.2 mm and 0.1 mm) calculations, the modified ENO scheme has produced reasonable and accurate one- and two-dimensional detonation waves (Hu *et al* 2002). However, some numerical instabilities occur near the incident wave front when the same scheme is used for high-resolution calculations. To eliminate these numerical errors, the more robust fifth-order WENO-LF scheme is used instead (Jiang and Shu 1996). The time discretization for the fluid dynamic terms is the third-order TVD Runge–Kutta method (Shu and Osher 1988). For the chemical kinetic integration, the set of coupled source terms is solved by the selected asymptotic integration method (Young 1979), which was used successfully in several detonation simulations (Oran and Boris 1987, Oran *et al* 1991, 1998). The time-step splitting scheme is used to couple the Euler equations to the chemical reactions (Oran and Boris 1987, Fedkiw *et al* 1997). The parallel virtual machine (PVM) technique is controlled and synchronized by PVM3.3, is used, in which the computations involved in the solution of the stiff ODEs on all grid nodes are divided into different computational zones and are spread among the different processors (Geist *et al* 1994).

2.1. Computational setup and initialization

The numerical simulation models a detonation propagating from left to right in a two-dimensional channel with a stoichiometric H_2/O_2 mixture diluted with 70% argon at an initial pressure and temperature of 6.67 kPa and 298 K, respectively. First, one-dimensional detonation is initialized by a strong shock wave and attains a mean detonation velocity of 1625 m s^{-1}, which is very close to the CJ value of 1618 m s^{-1} (Gordon and McBride 1971, Hu and Zhang 2002). Then, the solution is placed on a two-dimensional grid serving as the initial conditions for the two-dimensional calculation. According to our one-dimensional steady solution (see also Fickett and Davis 1979), the calculated reaction zone length is about 0.011 m, and the reaction-induced length is about 0.0016 m (which is defined as the distance from the shock front to the maximum heat release location). These results are only slightly smaller than those given by Oran *et al* (1998).

The right-hand boundary condition is kept in a quiescent state. As discussed in Gamezo *et al* (1999), the left-hand boundary condition is an extrapolated out-flow with a relaxation coefficient of 0.05. The boundary conditions imposed on the upper and lower boundaries reflect boundary conditions assuming that there is no energy loss to the channel wall. In order to keep the detonation front within the computational domain, the grid is set to move at a one-dimensional steady detonation velocity in the positive x-direction. Then the numerical detonation wave is thus observed for a very long physical time and is ascertained to be free from the effect of the initial condition with imposed perturbations. As Sharpe (2001) has suggested that the structure may show grid size effects when the grid size is comparable with or larger than the reaction zone length, very small grid sizes at least one to two orders smaller are used in the present calculations to minimize possible grid size effects. The grid size employed for calculating the formation process of the regular cellular structure is 0.2 mm. Then the results are projected onto half-size grids, which are 0.1 mm, 0.05 mm and 0.025 mm, by conservative interpolations. The smallest grid size is about one-sixth that of Oran *et al* (1998), which translates to about 440 node points for the reaction zone. In all these cases, the spatial discretization is the same for the x and y directions. The initial condition is perturbed by introducing random disturbances to the initial states only for the first time-step of chemical kinetic integrations via

$$e^* = e + \alpha e f. \tag{4}$$

Here, e^* is the perturbed total specific energy that encompasses small fluctuations imposed on the elementary reactions, f is a random value distributed uniformly in $[-1.0, 1.0]$ and α is a fluctuation coefficient, $0 < \alpha < 1.0$, controlling the fluctuation amplitude.

3. Formation of the regular structure

The numerical results show that the initial disturbances, with $\alpha = 0.3$, are very small and one can hardly distinguish the difference from the pressure contours calculated without the imposition of perturbations (see figure 1(*a*)). However, as the detonation propagates, the disturbances are magnified and many non-uniform regions are produced. It is further observed that the existence of transverse waves, Mach stems and incident waves, which eventually give rise to the triple-wave configuration, is clearly evident at about 15 μs (see figure 1(*b*)). These triple-wave configurations continue to move irregularly in the transverse direction. It is only after a very long time, about 1 ms later, that the structure becomes very regular with a lower transverse wave number. In the current work, the transverse wave number formed is found to be 5. Once the regular structure is reached, the detonation runs with the same transverse

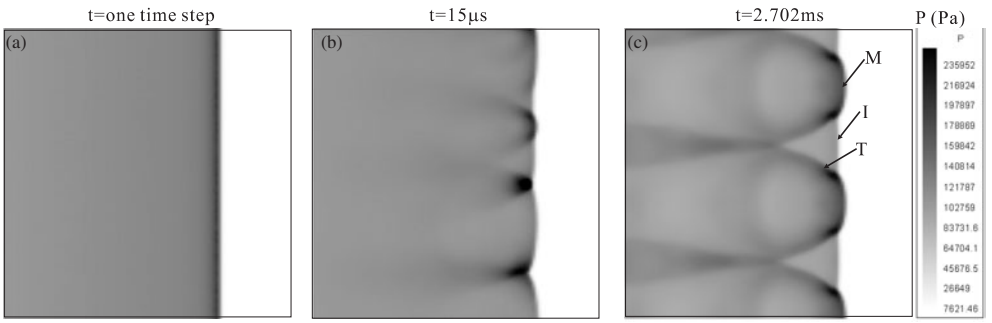

Figure 1. Pressure contours at three time points, channel height is 20 mm (notation in 1(*c*)—*T*, transverse wave; *M*, Mach stem; *I*, incident wave).

wave number for a further 3 ms, which is the longest time for the current computations. From our numerical experiments, it is also found that increasing the intensity of the initial perturbation with a higher value of α in equation (4), the time for the formation of the triple-wave configuration is shortened slightly. If α is smaller than 0.05, the fluctuations disappear after several microseconds. However, if α is sufficiently strong (even with a large α at 1.0) for leading to a cellular structure, the same mode regular structure is reached at almost the same time, provided the channel height is kept the same. These numerical experiments suggest that the final cellular structure is independent of the initial conditions. Figure 2 shows the detailed cellular structure in a 20 mm channel at time $t = 2.0728$ ms; in fact, the same structure occurs at about every 9.2 μs, which is called the characteristic time of the detonation cell, t_{char}. The transverse wave space, that is the cell width, computed in this case study is 0.008 m. It is also found that through the whole calculation, the average detonation velocity is maintained of 1625 m s^{-1}, which is the same as with the one-dimensional results.

4. Structures with different grid sizes

Figures 2 and 3 show the pressure, density, temperature and H_2O concentration of the structure with one transverse wave at time $t = 2.0728$ ms using grid sizes of 0.2 mm and 0.025 mm, respectively. In both cases, the structure is at about the half-way point location of two successive triple point collisions. At this location, the structure configuration has been developed fully from an earlier triple point collision.

For the results with a 0.2 mm grid size, which is approximately the same grid size as employed in previous studies with a detailed chemical reaction model (Oran *et al* 1991, 1998), the triple-wave configuration is shown. The detailed features around the triple point, however, are not so apparent. The position of the triple point is not sufficiently defined for the coarse resolution. There seems to be the presence of a slip line dividing the regions behind the Mach stem and the transverse wave, but again the features are not so clear or well defined (see figures 2(*b*) and 2(*c*)). Strictly, a transverse wave can be divided into two parts: one is the part connected to the triple-wave point called the main transverse wave; the other part extends from the main transverse wave and is called the extending transverse wave. However, the transverse wave seems to be extended from the triple-wave points smoothly, and there is no distinct turning point between the two parts (see figure 2(*a*)). Therefore, the configuration may look like a single-Mach configuration, which is one of the hallmarks of a weak structure. On the other

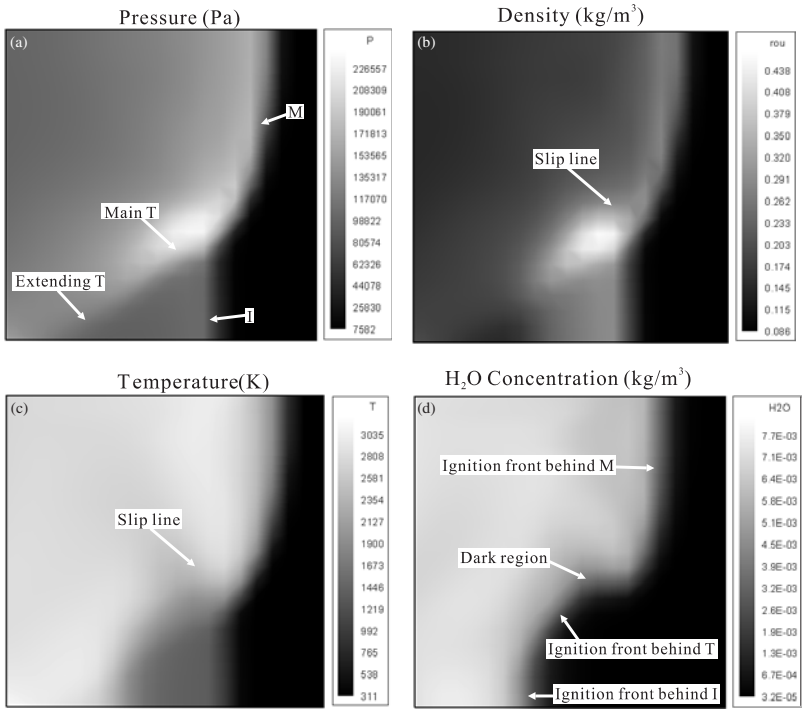

Figure 2. Structure with one transverse wave with 0.2 mm grid size at $t = 2.0728$ ms: (*a*) pressure, (*b*) density, (*c*) temperature, (*d*) H_2O concentration.

hand, the information obtained from the chemical reaction plot leads to a different conclusion. From the H_2O concentration contour, the ignition front can be defined approximately by the concentration discontinuity (see figure 2(*d*)). It can be observed that the Mach stem, the incident wave and the main transverse wave all contribute to ignition. This transverse wave ignition is the most notable characteristic of a strong structure. Furthermore, there is a perceptibly dark region behind the adjoining section of the Mach stem and the transverse wave can be observed (see figure 2(*d*)), which implies lagged ignition and indicates that a transversely moving weak wave exists ahead.

Figure 3 shows the detailed structure with a 0.025 mm grid size. For the purpose of analysis, the features of the structure are reproduced schematically in figure 4 according to the results presented in figure 3. It can be observed that the structure is much more complicated than that found on the coarse grid. The structure configuration is labelled as follows: I, M and T are the incident wave, the Mach stem and the whole transverse wave, respectively; S is the first slip line; RR stands for the approximated ignition front (H_2O concentration discontinuity in figure 3(*d*)); and a and b are the first and the second triple points; c is the kink that divides the main transverse wave and the extending transverse wave. In figure 4, the straight line section ab is a weak shock wave, called the weak transverse wave, whose strength is about 0.88 (defined as $S = p/p_o - 1$, in which p and p_o are the pressures across the front); the straight line section bc is the strong transverse wave front whose strength is about 1.70; the section of extending transverse wave front beyond the kink c is curved, and an expansion fan-like region around the kink can also be observed (see figure 3(*a*)). On the first slip line, S, the point d is the intersection with a shock wave bd (the additional shock wave). There is

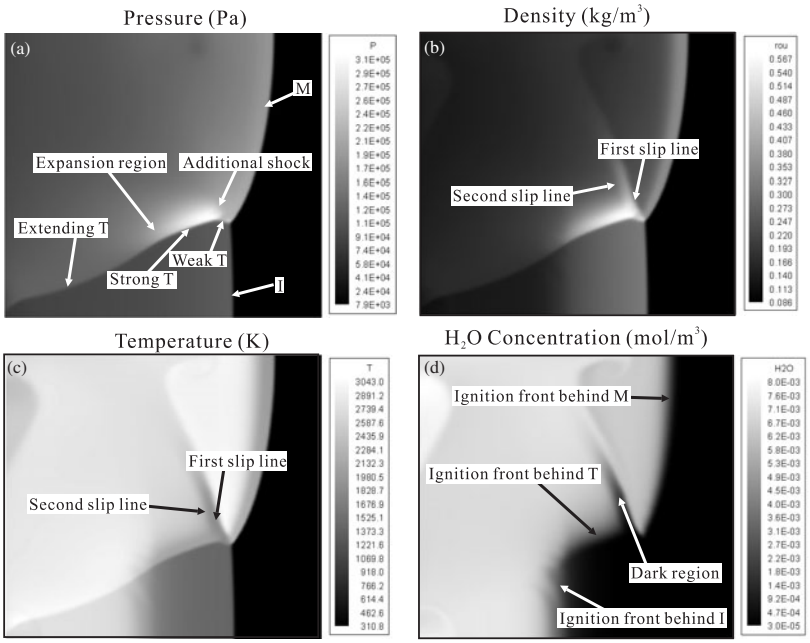

Figure 3. Structure with one transverse wave with a 0.025 mm grid size at $t = 2.0728$ ms: (*a*) pressure, (*b*) density, (*c*) temperature, (*d*) H_2O concentration.

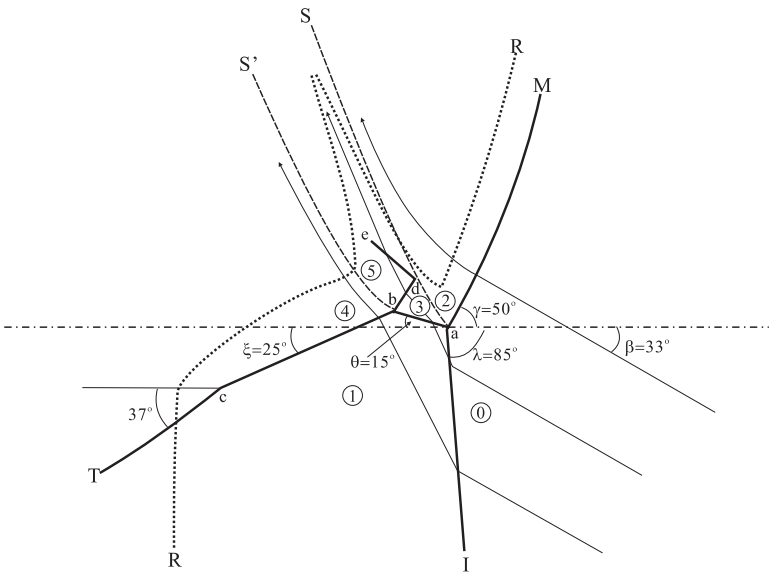

Figure 4. A schematic of the detailed configuration at $t = 2.0728$ ms with five regions as denoted by 1, 2, 3, 4 and 5. *RR* is the ignition front and *S* and *S′* are the first and the second slip lines.

another weak shock wave *de*, which is the reflection wave of the additional shock wave *bd* off the slip line *S*. Between the additional shock wave, *bd*, and the strong transverse wave, *bc*, there is also a weak slip line *S′* called the second slip line, which is clearly shown in figure 3(*c*) of the temperature plot and figure 3(*d*) of the H_2O concentration.

Table 1. Properties of the structures at different resolutions.

Grid size $\Delta x = \Delta y$	Transverse wave parts	Slip line number	Triple-wave point number	Additional shock wave
0.2 mm	2	1	1	No
0.1 mm	3	1	2	No
0.05 mm	3	2	2	Yes
0.025 mm	3	2	2	Yes

The above wave configuration resembles to some extent that of a double-Mach reflection of a shock wave. The main difference between them is that there is no kink *c* for the latter. For a non-reactive shock wave, a kink occurs at the reflection wave of the transitional-Mach configuration. This suggests that the second triple-wave configuration in the cellular structure is transitional-Mach-like. Therefore, the whole structure shows greater strength than a merely double-Mach configuration. Generally, five regions can be classified according to the observed structure: region 0 is the area ahead of the Mach stem and the incident wave; region 1 is the area behind the incident wave and ahead of the strong transverse wave; the area behind the Mach stem and the weak transverse wave is divided into region 2 and region 3 by the first slip line; the area behind the strong transverse wave and the additional shock wave is divided into region 4 and region 5 by the second slip line (see figure 4).

The ignition front *RR* shows stronger ignition behind the Mach stem and the strong transverse wave but weaker ignition behind the incidental wave (see figure 4). This is because the induced length (the normal distance from ignition front to leading shock wave) behind the incident wave is much longer than that behind the Mach stem and the strong transverse wave, *bc*. It can also be observed that the gas mixture behind the Mach stem is burned by Mach stem ignition, while the gas mixture behind the incident wave is ignited by the incident wave and the strong transverse wave, *bc*. The weak transverse wave, *ab*, the additional shock wave, *bd*, and its reflection wave, *de*, off the first slip line are so weak that the ignition of the induced zones behind them is greatly lagged relative to the strong transverse wave and forms the so-called lagged region. The ignition behind the lagged region, as the horizontal induced length behind is shorter, is stronger than that of the incident wave. In general, it may be suggested that all the ignitions behind the Mach stem, the incident wave and the transverse wave are associated with strong shock-induced ignition processes. The extending transverse wave does not contribute to ignition since its front is behind the ignition front (see figure 3(*d*)). Furthermore, there is the fairly distinct kink, point *c*, which divides the main transverse wave. From the above descriptions, the structure shown is clearly of a multi-Mach configuration with more than one triple point and the presence of strong transverse wave ignition.

It may just be noted that the calculation made with the modified third-order ENO-LLF scheme for the 0.025 mm grid size yields results very similar to those of the fifth-order WENO scheme shown in figure 3, except for some limited oscillations observed near the induced region associated with the incident front. Furthermore, the calculated results with grid sizes 0.1 mm and 0.05 mm show with increasing clarity that the detailed structure is characterized by a multi-Mach configuration (not presented here). Therefore, one can conclude that the cellular structure is of the strong type. Other unchanged detonation parameters obtained are the global features such as the average detonation velocity and the transverse wave space or cell width, hence suggesting independence of the numerical schemes and grid sizes. Of course, the structure shows different levels of detail when different grid sizes are employed. Some selected features of the structure with different resolutions are given in table 1 for comparison. These results also show good convergence for the features of the structure with increasing spatial

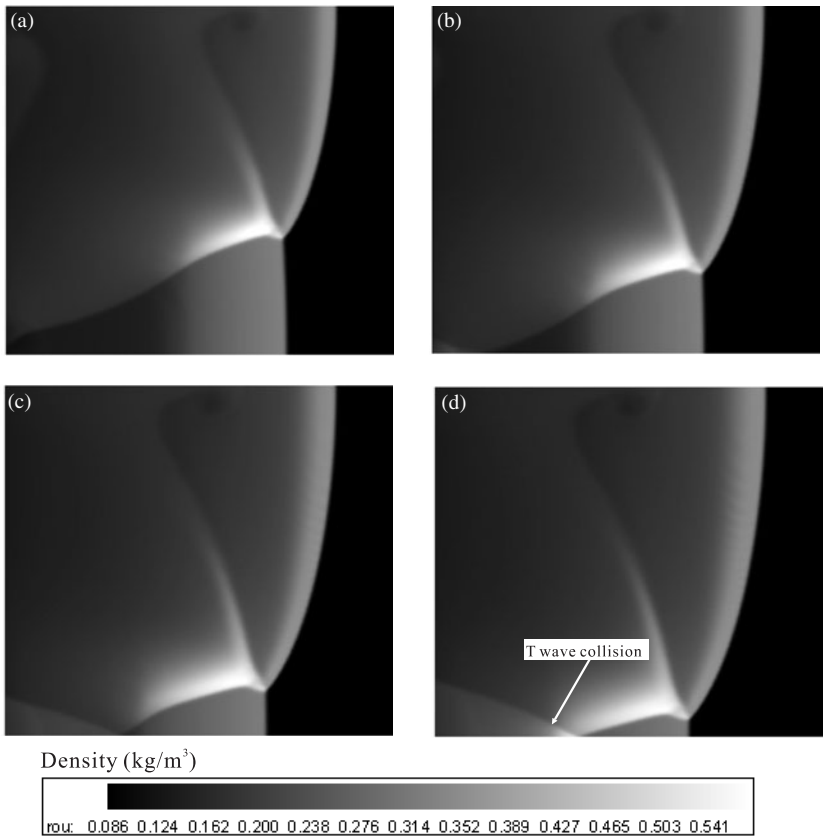

Figure 5. Density for the structure with one transverse wave at four successive snapshots before the triple collision: (*a*) $t = 2.0728$ ms, (*b*) $t = 2.0732$ ms, (*c*) $t = 2.0736$ ms, (*d*) $t = 2.0740$ ms.

resolution. Lastly, it may be reiterated that for the coarse grid of 0.2 mm or for a 0.1 mm grid size, many of the structure details are lost, especially those near the second triple point.

5. Evolution of the structure

In the structure, the Mach stem and the incident wave interchange their roles via the Mach/triple point collision as the detonation proceeds forward. Therefore, it is convenient to divide the structure evolution process into three parts: before, through and after the triple point collision.

5.1. Before the triple point collision

Figures 5 and 6 show the density and H_2O concentration at four successive time points: (*a*) 2.0728 ms, (*b*) 2.0732 ms, (*c*) 2.0736 ms and (*d*) 2.0740 ms. The last snapshot is just before the triple point collision occurs. Table 2 gives the change of states in the structure (i.e. for the five regions indicated in figure 4) in the period between $t = 2.0728$ ms and $t = 2.074$ ms, showing the variation of the structure from the fully developed state after an earlier triple point collision (see figure 3) to the time just before the next collision occurs. The overall feature

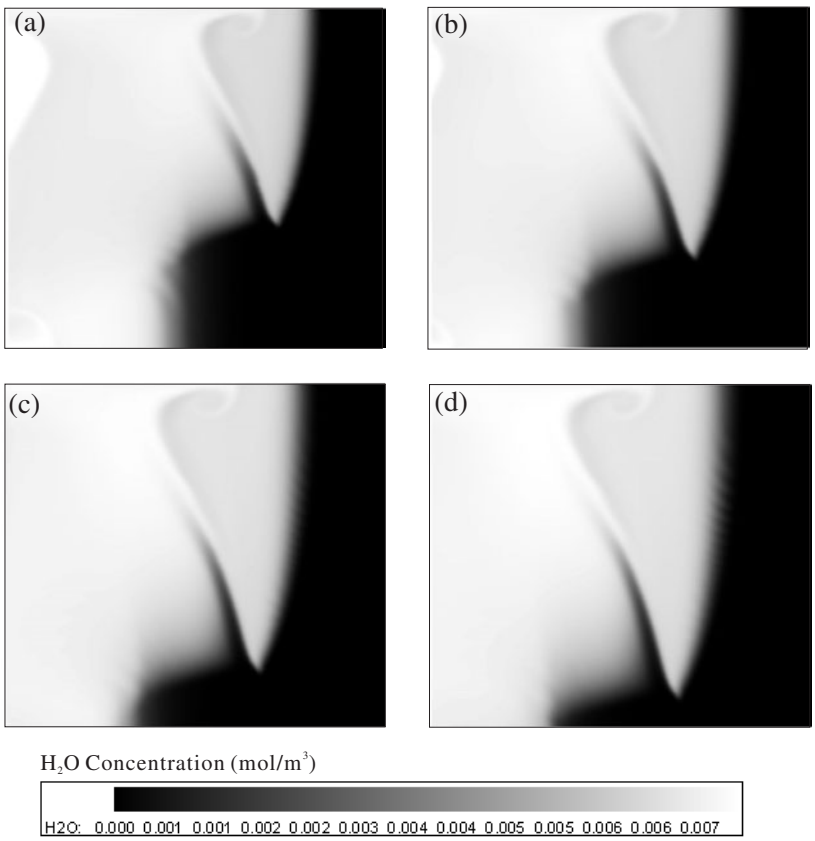

Figure 6. H_2O concentration for the structure with one transverse wave at four successive snapshots before the triple point collision: (*a*) $t = 2.0728$ ms, (*b*) $t = 2.0732$ ms, (*c*) $t = 2.0736$ ms, (*d*) $t = 2.0740$ ms.

Table 2. Change of state in the structure before the triple point collision.

Region	1	2	3	4	5
p/p_o	18.5 → 16.3	34.8 → 30.3	34.8 → 30.3	49.9 → 40.5	49.9 → 40.5
ρ/ρ_o	3.73 → 3.56	4.28 → 4.21	5.57 → 5.45	6.73 → 6.31	6.91 → 6.63
$T(K)$	1470 → 1256	2367 → 2160	1856 → 1661	2195 → 1928	1993 → 1837

Table 3. Angle changes for wave fronts in the structure before the triple point collision. All angles are measured with respect to the invariant horizontal axis (see figure 4).

	Track (β)	M (γ)	I (λ)	T_{weak} (θ)	T_{strong} (ξ)
Angle (°)	33 → 39.5	50 → 44.5	85 → 90	15 → 20	25 → 20

of the structure is that the strength of both the Mach stem and the incident wave decreases. The strong transverse wave decreases in strength from 1.8 to 1.5, but the strength of the weak transverse wave shows only a small change. While the structure evolves towards the collision, the configuration looks like having been rotated clockwise by about 5° around the first triple-wave point (see table 3), and the relative angles between the wave fronts themselves have not

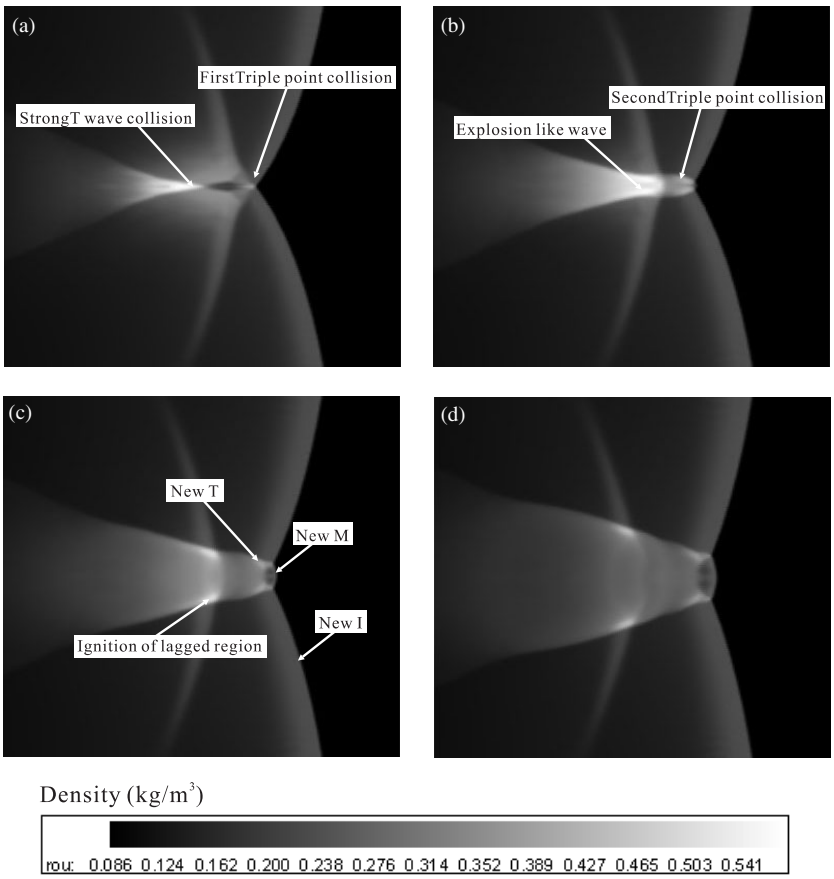

Figure 7. Density at four successive snapshots through the collision of two configurations: (*a*) $t = 2.0742$ ms, (*b*) $t = 2.0744$ ms, (*c*) $t = 2.0746$ ms, (*d*) $t = 2.0748$ ms.

changed much. In essence, the angle that the whole configuration has rotated is just about equivalent to the deflection of the triple point track angle, β, varying from 33° to 39.5°. It can be observed that the distance from the leading front to the ignition front has been extended because of the decay of both the Mach stem and the incident wave. The area of the lagged region behind the weak transverse wave is also increasing gradually and makes a long dark triangle region (see figure 6(*d*)). It is also noted that the extending transverse wave (i.e. the section of transverse wave beyond kink *c* in figure 4) collides before the occurrence of the triple point collision (see figure 5(*d*)).

5.2. Through the triple point collision

Figures 7 and 8 show the density and H_2O concentration, respectively, at four different time points, (*a*) 2.0742 ms, (*b*) 2.0744 ms, (*c*) 2.0746 ms and (*d*) 2.0748 ms, through the triple point collision. It can be observed easily that the collision is a symmetric one and in turn can be broadly divided into four successive processes: the strong transverse wave collision, the first triple point collision, the second triple point collision and the formation of the new Mach configuration.

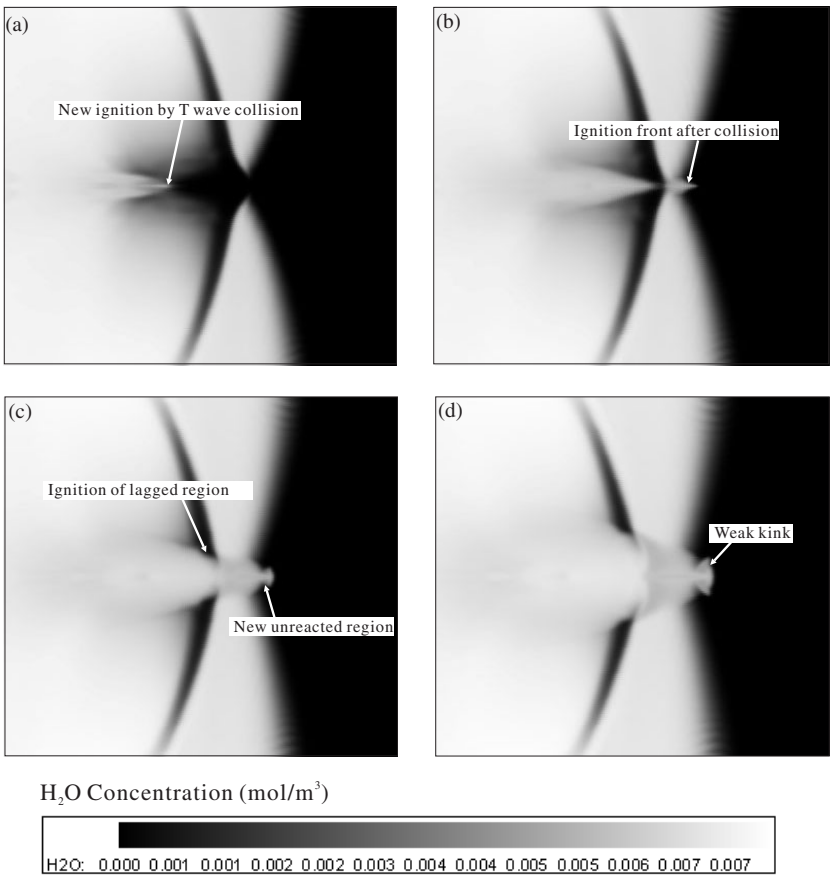

Figure 8. H_2O concentration at four successive snapshots through the collision of two configurations: (*a*) $t = 2.0742$ ms, (*b*) $t = 2.0744$ ms, (*c*) $t = 2.0746$ ms, (*d*) $t = 2.0748$ ms.

As mentioned in the last section, before the triple point collision occurs, the extending transverse wave starts to collide without leading to ignition as it occurs behind the ignition front of the incident wave. When the two transverse waves move close enough, the strong transverse waves collide within the induced length of the incident wave. As the angle between the two strong transverse waves is only about 40°, the collision is a regular one and makes a new ignition front with a triangle shape (see figures 7(*a*) and 8(*a*)). The collision centre has a very high pressure at about 660 kPa and behaves like an explosion wave (see figure 7(*b*)). While the strong transverse wave collides, the first triple point collision occurs (see figure 7(*a*)). It can be suggested that this latter collision is not a generally accepted Mach collision process (Fickett and Davis 1979) but a regular collision process of the two Mach stems. This is because the ignition front after the collision also shows a triangle shape (see figure 8(*b*)) similar to that of the regular strong transverse wave collision. If the collision is a Mach collision, the ignition front should be perpendicular to the collision line for a new vertical Mach stem produced. Following the strong transverse wave collision, the second triple point collision occurs subsequently and creates almost two normal colliding waves as the angle between the wave front is very small. After the above three regular collision process, a new Mach stem and the two new transverse waves are formed, and the structure can be considered as two new

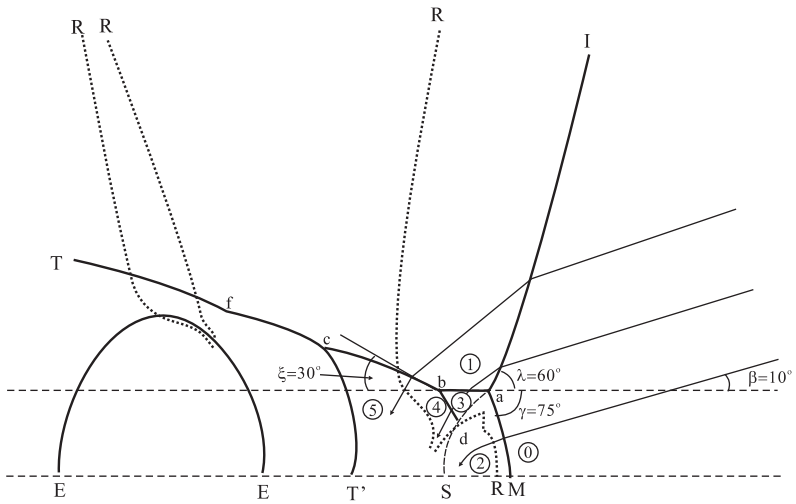

Figure 9. A schematic of the detailed configuration at $t = 2.0748$ ms. T' is the front of the explosion-like wave, and *EE* is the rarefaction region of the explosion-like wave.

Table 4. Change of state in structure through the triple point collision.

Region	1	2	3	4	5
p/p_o	$16.3 \rightarrow 25.4$	$30.3 \rightarrow 45.6$	$30.3 \rightarrow 45.6$	$40.5 \rightarrow 58.9$	$40.5 \rightarrow 58.9$
ρ/ρ_o	$3.56 \rightarrow 4.0$	$4.21 \rightarrow 4.28$	$5.45 \rightarrow 6.08$	$6.31 \rightarrow 6.45$	$6.63 \rightarrow 6.62$
$T(K)$	$1256 \rightarrow 1903$	$2160 \rightarrow 3107$	$1661 \rightarrow 2370$	$1928 \rightarrow 2648$	$1873 \rightarrow 2512$

Table 5. Angle changes for wave fronts in the structure through the triple point collision.

	Track (β)	M (γ)	I (λ)	T_{weak} (θ)	T_{strong} (ξ)
Angle (^{o})	$39.5 \rightarrow 10$	$44.5 \rightarrow 75$	$90 \rightarrow 60$	$20 \rightarrow 0$	$20 \rightarrow 30$

double-Mach-like configurations lying symmetrically about the collision line (see figures 7 and 8). It is hard to define an intervening weak structure or single-Mach configurations between the regular collisions and the double-Mach-like configuration. Meanwhile, the explosion-like wave of the new ignition region caused by transverse wave collision decays quickly. However, as it encounters the lagged regions and ignites them, new pressure peaks are produced around the ignition front of these lagged regions (shown as density peaks in figures 7(c) and 7(d)). It can also be observed that once the double-Mach-like configuration is formed, new lagged regions are produced behind the new transverse waves (see figure 7(c) and 8(c)).

Figure 9 gives a schematic of the structure in accordance with the results of figures 7(d) and 8(d). Tables 4 and 5 show the change in the respective states and the wave front angles in the structure through the triple point collision. It can be observed that the structure configuration bears some similarities to figure 4. There is an explosion-like wave front T' that has become weak by this time and changed to a compressive wave, thereby giving rise to a low pressure rarefaction region encircled as *EE* (figure 9). No (obvious) kink point dividing the main transverse wave and the extending transverse wave is observed. Actually, the extending transverse wave is still developing and its front is different from that in figure 4. Comparing with the structure before the triple collision, it can be suggested that the new incident wave, I,

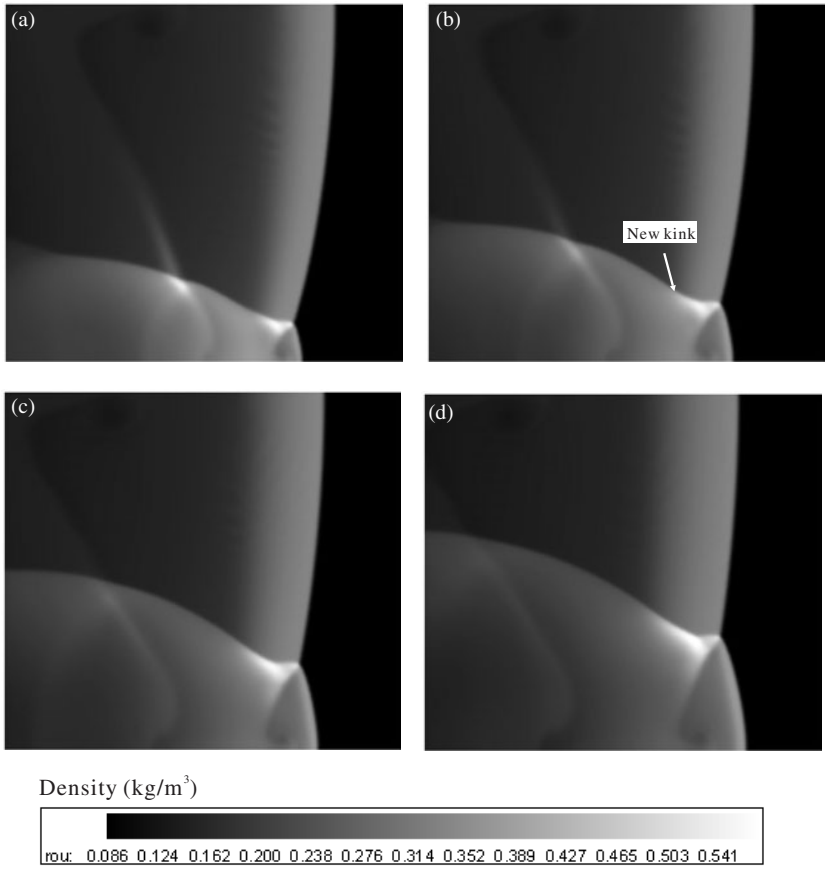

Figure 10. Density at four successive snapshots after the triple point collision: (*a*) $t = 2.0752$ ms, (*b*) $t = 2.0756$ ms, (*c*) $t = 2.0760$ ms, (*d*) $t = 2.0762$ ms.

has a smaller front angle, and the new Mach stem has a larger front angle, while both of them are stronger. The newly developed transverse wave, T, is also stronger and shows a more complicated front configuration. The weak transverse wave front, ab, is almost parallel to the collision line, and the new track angle is only about 10°. However, the shape of the configuration has not changed much for the acute angle between the Mach stem and incident wave remains at about 45°, which is very close to that before the collision (see and compare tables 5 and 3).

5.3. After the triple point collision

Figures 10 and 11 show the density and H_2O concentration of the upper part of the structure after the triple point collision at four successive time points: (*a*) 2.0752 ms, (*b*) 2.0756 ms, (*c*) 2.0760 ms and (*d*) 2.0762 ms. As the structure evolves further, the kink point between the extending transverse wave and the strong transverse wave is formed once again, and the extending transverse wave front develops into a curved line (see figure 10(*b*)). The main transverse wave front also becomes longer via ignition of more areas of the induced zone behind the incident wave. The weak transverse wave front lengthens, and the area of the new lagged

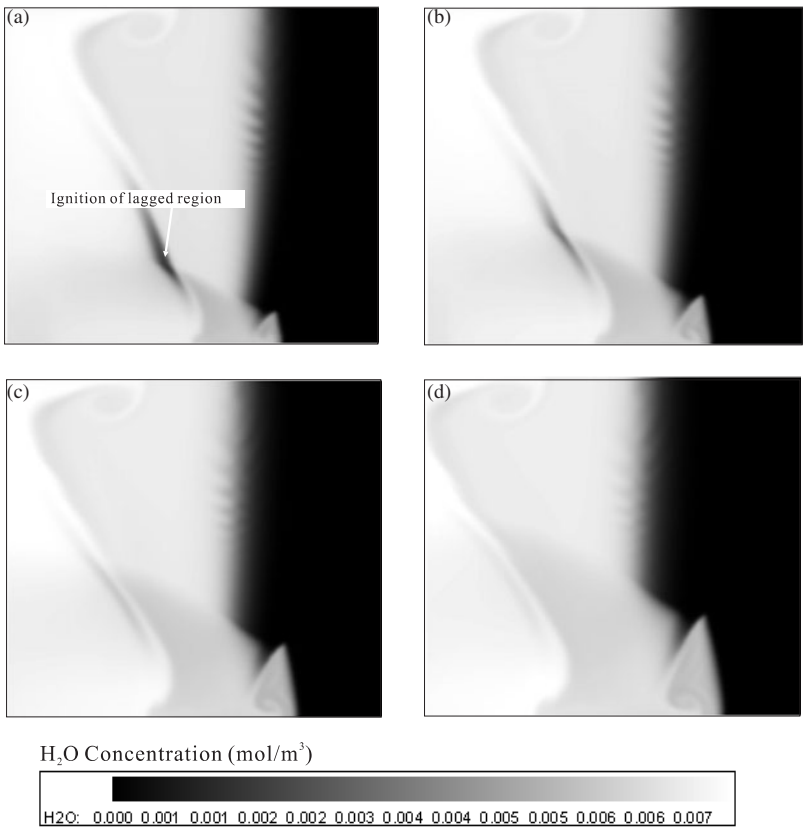

Figure 11. H_2O concentration at four successive snapshots after the triple point collision: (*a*) $t = 2.0752$ ms, (*d*) $t = 2.0756$ ms, (*c*) $t = 2.0760$ ms, (*b*) $t = 2.0762$ ms.

region also increases. The lagged region left by the structure before the collision is ignited by the colliding transverse wave (see figures 11(*b*) and (*c*)). As the structure evolves further, it becomes and tends towards the states as shown previously in figures 5 and 6. Generally, it may be noted that, after the triple point collision, the overall relative configuration changes little except for the Mach stem and the incident wave, which have their shock pressure decreased. On the other hand, the transverse wave strength does not change much. It can also be found that the overall configuration rotates by approximately 20–25° counterclockwise in the period from $t = 2.0748$ ms to $t = 2.077$ ms, which is opposite (clockwise) to the rotation before the triple collision. Meanwhile, the triple point track angle, β, changes from 10° to 33°.

6. Structure tracks

The smoke foil technique has been used widely to study the tracks of the structure. Usually, a high speed flow can remove more soot than the lower speed counterpart, and so the tangential velocity discontinuity on the slip line is recorded dividing the regions behind the Mach stem and the transverse wave in a triple-wave configuration. Similarly, in the present work, the maximum flow velocities, $|\boldsymbol{v}|_{\max}$, on all grid nodes in the time history are recorded to simulate

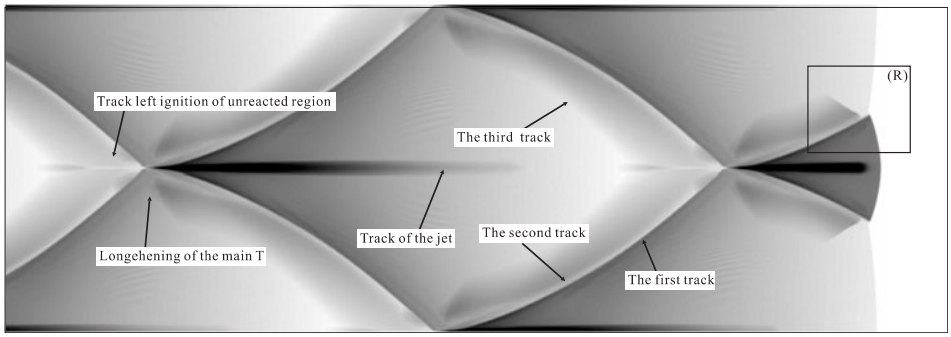

Figure 12. Numerical detonation cells in a 8 mm channel (region (R) is shown schematically in figure 13).

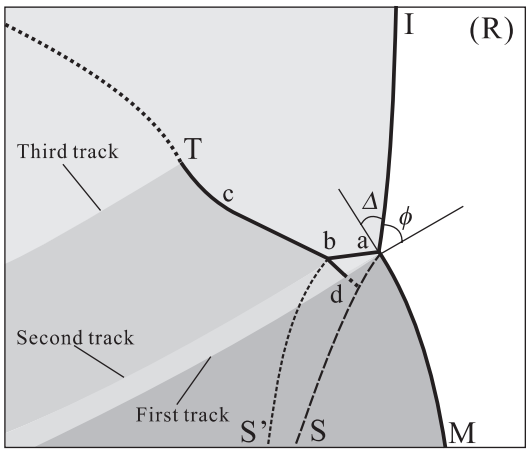

Figure 13. The making of structural tracks in a numerical detonation cell.

the smoke foil tracks. That is,

$$|\boldsymbol{v}|_{max,i,j} = \left[\left(\sqrt{u^2 + v^2}_{i,j}\right)\right]_{\max}, \qquad t = 0, t_{\text{end}}. \tag{5}$$

Figures 12 and 13 show the numerical detonation cells as an analogue of smoke foil tracks and how the tracks are left after the sweeping of the structure, respectively. As with the experiment on the detonation cell, the numerical cell has convex curvature tracks in the first half cell and concave tracks in the second half cell. Generally, it can be observed that there are three tracks left by the structure (see figure 13). The first track is left by tangential velocity discontinuity on the first slip line, S; this is associated with the strong velocity discontinuity between the regions behind the Mach stem, I, and the weak transverse wave, ab. The second track is left by the tangential velocity discontinuity on the second slip line, S' (which pertains to the velocity discontinuity between the regions behind the main transverse wave, bc, and the additional shock wave, bd). The third track is left by the region near the kink point, c, to the extending transverse wave. By comparing with the structure details in figure 3(d), it can be found that this region corresponds to the intersection area of the ignition fronts behind the strong transverse wave and the incident wave. Of the three tracks, the first track is the strongest due to the largest velocity discontinuity between the first slip line. The third track is the weakest for its weak expansion-like configuration, which gives rise to an almost continuous transition (see also figure 12).

The third track around the triple point collision shows the lengthening process of the strong transverse wave front with increasing area of the induced zone behind the incident wave. The track left by the forward jet at the cell apex is shown clearly in the numerical detonation cell, and there are also weaker and smaller tracks just before the triple point collision, suggesting the leftover lagged regions of the structure have been ignited (previously) by the regular collision of transverse waves (see figure 12).

7. Comparison with experiments and previous calculations

As strong structures can be observed directly in a marginal detonation, it is straightforward to compare them with the structure simulated in this work. The current numerical structure bears several characteristics in common with the experiments involving schlieren photographs of marginal planar and rectangular cellular detonations by Voitsekhovskii *et al* (1963). There are the presence of the two triple points *a* and *b* and the two slip lines *S* and *S′*. Both numerical and experimental results show that the weak transverse wave front is short compared to the strong transverse wave. The present lagged region behind the weak transverse wave is also consistent with previous experiments and simulations on marginal detonations (Subbotin 1975, Gamezo *et al* 2000). In the reconstructed structure from marginal detonation experiments in low pressure $H_2/O_2/Ar$ mixtures by Strelow and Crooker (1974), the third and the fourth triple points are reckoned to be present around the region of the intersection of ignition fronts behind the strong transverse wave and the incident wave, with the third structure track fairly clear and so for the fourth. It is noted that the 'second' track of a marginal detonation in Strehlow and Crooker (1974) seems to have been left by the region between the third and the fourth triple points rather than by the second triple point as suggested by Sharpe (2001). These third and fourth triple points are not found in the current computation; instead an expansion wave-like configuration showing much weaker waves is present. The current calculated strength of the strong transverse wave is also only about one-third that of Voitsekhovskii *et al* (1963). This indicates that the structure is much weaker than that of the marginal detonation structure obtained from experiments. Oran *et al* (1998) did simulations with a detailed chemical reaction model using grid sizes of about 0.2 mm and also suggested the presence of a strong structure. However, the structure configuration is not so well defined, possibly due to the coarse resolution, especially so for the wave fronts around the second triple point. Sharpe (2001) simulated the structure with a simple reaction model. He also obtained a strong structure but with a much longer and weaker transverse wave front. The present fairly-straight-line feature of the strong transverse wave beyond the second triple point is not found in Sharpe's results, but instead evidence of a smooth curved front without the kink dividing the strong and extending transverse waves is found. Sharpe's results resemble closely the configuration of a double-Mach reflection and suggest that the strength of the strong transverse wave is fairly weak. This is further supported by the incomplete chemical reaction behind it. Strictly, the results obtained by Sharpe can be considered to be more indicative of a weak structure because of the much less intense ignition ability of the strong transverse wave. Another difference between Sharpe's results and ours is that the former obtained a strong kink at the Mach stem. In the current result, it only exists in a weak form near the first triple point just after the triple point collision (see figure 8(*d*)). This strong kink has also not been found in experiments and other numerical simulations with a detailed chemical reaction model; it has been found in other high resolution numerics with a simple chemical reaction model (Quirk 1993, Zhang *et al* 2001), which may suggest that the selection of the chemical reaction model has important effects.

As discussed, besides the seemingly small number of triple points and weaker transverse wave strength as compared with a marginal detonation, the chemical reaction mechanisms of

the present strong structure are also different. Mitrofanov (1996) reconstructed the marginal detonation ignition mechanisms from experiments in which the gas mixture could not be ignited directly by the incident wave but by the so-called third shock compression caused by colliding transverse waves. However, the present results show that shock-induced ignition occurs ahead of the transverse wave collision unless the two transverse waves are so close and lead to collision within the induced length behind the incident wave. In marginal and irregular detonation structures, unburnt pockets are observed in experiments and numerical simulations (Subbotin 1975, Gamezo *et al* 1999). These unburnt pockets are ignited behind a long induced length, the longest of which is about the order of the cell length. These unburnt pockets are different from the lagged regions just after the triple point collision in the present simulation. The main difference is that the current lagged regions are ignited much more quickly. The longest induced length is only about one-tenth the cell length and close to that of the incident wave. The existence of unburnt pockets is suggested as one of the main dissipation mechanisms that make the detonation velocity considerably lower than D_{CJ} or even extinction (Oran *et al* 1991). However, the lagged region in the present work may not have the same effects since the average detonation velocity is the same as in the results from the one-dimensional state and very close to D_{CJ}.

Through the structure evolution, the acute angle between the weak incident wave and the transverse wave track (ϕ) is in the range 45–50°; the acute angle between the incident wave and the Mach stem (Δ) is in the range 40–45°. Furthermore, the angle between the Mach stem and the first track is almost constant and very close to 90° (see figures 12 and 13). By comparing the pressure ratio across the transverse wave, the transverse wave strength is found to be in the range 1.5–1.8 for the strong transverse wave and almost constant at about 0.8 for the weak transverse wave. One can find that these results bear some similarities to those of Urtiew (1976). That is, the angle ϕ and the transverse wave strength are approximately constant through the cell, and the configuration can be considered as an object with a fixed shape moving along the cell track and rotating to keep ϕ constant. According to the qualitative picture provided by Strehlow and Crooker (1974), just after the triple point collision, the structure appears to be a weak type and evolves to become a strong type. The numerical results of Lefebvre and Oran (1995) and Oran *et al* (1998) have also suggested that the structure begins as a weak type and changes to the strong type gradually. However, as pointed out by Fickett and Davis (1979), the event taking place through the process and just after the triple point collision for the experiments is still unclear since details are hardly resolved due to the very short space scale and timescale of both the reaction and flow. Lefebvre and Oran's (1995) analysis is based on a coarse grid and may also encounter similar difficulties as in the experiments. Therefore, it is reckoned that only with numerical results with sufficiently high time and spatial resolutions is it possible to verify the fine process of the whole triple collision, deemed not possible with the current state-of-the-art experiment. The present simulation indicates that the structure just after the collision depicts a regular collision configuration. Furthermore, it shows the structure changing quickly to a double-Mach-like configuration, which is of a typical strong type. Sharpe (2001) showed that the triple collision is similar to a double-Mach reflection process. A possible reason for this is that the simple chemical reaction model employed is still able to resolve some aspects of the structure-related chemical reaction but not all the finer features. The calculated strong transverse waves are too weak and make the collision process resemble a collision of two non-reaction shock waves.

The present average detonation speed is $1625\,\mathrm{m\,s^{-1}}$, which implies a typical ordinary detonation property. Other comparisons of parameters between the present simulation and experiment for ordinary detonation are provided in table 6, showing reasonable concurrence. For the transverse wave strength, the results from experiments are closer to that of the simulated

Table 6. Comparisons of parameters between simulation and experiments of ordinary detonations

Parameters	Numerical simulation	Experiments[a]
Mean detonation velocity ($\bar{D}/D_{CJ}$)	1	~ 1
Variation through the cell (D/D_{CJ})	1.43–0.77	1.2–0.85
Transverse wave strength (strong/weak)	1.7, 0.8	~ 0.5

[a] From Fickett and Davis (1979).

weak transverse wave. This can perhaps be attributed to the experimental result being deduced and evaluated indirectly based on the hypothesis that the triple point collision is of two identical single-Mach structure collisions (Strehlow and Biller 1969). On the other hand, experiments on chemical reactions pertaining to the structure have also provided other indirect evidence of the presence of a strong structure in ordinary detonations. Voitsekhovskii *et al* (1963) pointed out that the transverse wave can lead to strong ignition, as recorded by their light radiation. Our simulation shows very strong ignition behind the strong transverse wave, which is even more intense than that behind the incident wave, and hence the possibility of the strong transverse wave leading to strong ignition with light radiation.

As the structure evolves, the instantaneous detonation velocity reaches its maximum during a triple point collision and then decays to its minimum before the next triple collision. The present detonation velocity fluctuation is about $1.43–0.77 D_{CJ}$. In the results of Oran *et al* (1998), the calculated overall velocity fluctuation/variation is about $1.38–0.85 D_{CJ}$, which is slightly smaller than the present results. Compared with the experimental detonation velocity fluctuations, both simulations show the triple collision is stronger than that of an ordinary detonation but not as severe as that of a marginal detonation. The present ratio of maximum to minimum detonation velocities is about 1.86. With the relation given in Urtiew (1976), this ratio is calculated to be about 1.7. These ratio values are also larger than 1.4 of an ordinary detonation but smaller than about 2.0 of a marginal detonation (Fickett and Davis 1979). Regarding the disagreements of this ratio value with the experimental data of an ordinary detonation, these may be attributed to the low resolution velocity measurement. Usually, the velocity measurement can only reflect the local average value; the very rapid velocity fluctuation region near the triple collision may not be captured faithfully and is likely to be underestimated compared with the slower process in other parts of the cell. This is similar to the fact when the detonation is calculated with a much lower resolution in both time and space, a smaller detonation velocity maximum is obtained. For example, in the present work, the calculated detonation velocity maximum is only about $1.35 D_{CJ}$ with a grid size of 0.2 mm. In work of Oran *et al* (1998), it was also observed that the maximum energy release associated with the finer grid calculation is much larger than that of the coarser grid counterpart. The former tends to form a stronger Mach stem with a higher speed leading front after the triple collision. It may be noted that to explain the disagreements between numerical results and experiments, Lefebvre and Oran (1995) and Oran *et al* (1998) suggested the presence of a mixed marginal and ordinary behaviour based on the ordinary detonation characteristic of having only a weak structure.

In our simulation, very clearly defined structure tracks are obtained, and the detonation cells show fairly good agreement with the experiments. The width/length ratio and track angles are close to those measured from the experimental detonation cells of the same gas mixture. Table 7 shows the details of comparisons between the numerical simulations and experiments (Strehlow 1968). Strehlow's (1969) argument for the presence of weak structures in ordinary detonations is based on the premise that the observed structure tracks are 'single lines'. However, if the experimental smoke foil tracks in Strehlow (1968) are analysed further,

Table 7. Comparison of cell geometries between simulation and experiments.

Cell geometries	Current results	Experiments[a]
Width/length (d/l)	0.55	0.5–0.6
Exit angle (β)	$<10^{\circ}$	5°–10°
Entrance angle (α)	40°	32°–40°
Track angle (ω)	30°	$\sim 30^{\circ}$

[a] From Strehlow (1968).

the 'single line' is actually a narrow band. In this band, less soot is removed compared with the neighbouring regions. This narrow band is very similar to the narrow band reflected in figures 12 and 13 and recorded by the region lying between the first and the second tracks. The third track calculated has not been observed in experiments. However, Strehlow and Crook (1974) showed that even for marginal detonation, where the structure is typically of the strong type, the 'second' track does not always leave its mark on the smoke foil. Therefore, for the much weaker third track in the present results, it is also very possible that it does not have sufficient intensity to be recorded by the smoke foil; only the two stronger, first and second, tracks are detected. Overall, the concurrence of the simulation and experiment suggests the presence of a strong structure for an ordinary detonation in a $H_2/O_2/Ar$ mixture. As many experimental smoke foil data (Fickett and Davis 1979) for *different* ordinary detonations show that the structure tracks are actually narrow bands too, it may be surmised that strong structures exist for other reactive systems.

8. Concluding remarks

In this paper, a two-dimensional simulation of the structure of a cellular detonation of a $H_2/O_2/Ar$ mixture has been performed with a detailed chemical reaction model. In the simulation, the regular structure is first produced about 1 ms after the introduction of small perturbations only at the first time step. The calculations have been carried out with different grid sizes. Good convergence features have been found, and a very high resolution structure has been produced with a grid size of 0.025 mm.

The calculated results suggest a strong structure with a double-Mach-like configuration, and transitional-Mach-like waves around the second triple point. As the structure evolves, the shape of the configuration remains almost unchanged but rotates around the first triple point. The triple point collision has been observed to comprise three successive regular collision processes, and the regular collision configuration changes quickly to a double-Mach-like one. These results have not been found in calculations with a coarser grid or simple chemical reaction models. Overall, the comparison with various experiments suggests that the present simulated structure is that of an ordinary detonation. Because the presence of a strong structure is also typically found in marginal detonations, the existence of a strong structure in any detonation detected cannot be used as the criterion for determining the type of detonation present. On the other hand, since the marginal detonation has much stronger transverse waves than that found for an ordinary detonation, it is suggested that the strength criterion of the transverse wave can be incorporated with others to determine the type of detonation encountered.

References

[1] Fedkiw R P, Merriman B and Osher S 1997 High accuracy numerical methods for thermal perfect gas flows with chemistry *J. Comput. Phys* **132** 175–90

[2] Fickett W and Davis W C 1979 *Detonation* (Berkeley, CA: University of California Press)
[3] Gamezo V N, Desbordes D and Oran E S 1999 Formation and evolution of two-dimensional cellular detonations. *Combust. Flame* **116** 154–65
[4] Gamezo V N, Vasil'ev A A, Khokhlov A M and Oran E S 2000 Fine cellular structures produced by marginal detonations *Proc. Combust. Inst.* **28** 611–17
[5] Geist A, Beguelin A, Dongarra J, Jiang W, Manchek R and Sunderam V 1994 *PVM 3 User's Guide and Reference Manual* ORNL/TM-12187
[6] Gordon S and McBride B J 1971 Computer Program for Calculation of Complex Chemical Equilibrium Compositions, Rocket Performance, Incident and Reflected Shocks, and Chamman-Jouget Detonations *NASA SP273*
[7] Hu X Y and Zhang D L 2002 Numerical simulation of gaseous detonation of H_2/O_2 mixture with detailed chemical reaction model *Explosion Shock* **22** 1–8 (in Chinese)
[8] Hu X Y, Khoo B C, Zhang D L and Jiang Z L 2002 Numerical studies on the reaction zones in a detonation wave with a detailed chemical reaction model *Computational Fluid Dynamics 2002* ed S Armfield *et al* (Berlin: Springer) p 502
[9] Jiang G S and Shu C W 1996 Efficient implementation of weighted ENO schemes *J. Comput. Phys* **126** 202–28
[10] Lefebvre M H and Oran E S 1995 Analysis of shock structures in regular detonation *Shock Waves* **4** 277–83
[11] Mitrofanov V V 1996 Modern view of gaseous detonation mechanism *Progress in Astronautics and Aeronautics* vol 137 (Washington, DC: AIAA) p 327–39
[12] Oran E S and Boris J P 1987 *Numerical Simulation of Reactive Flow* (New York: Elsevier)
[13] Oran E S, Boris J P and Kailasannath K 1991 Studies of detonation initiation, propagation and quenching *Prog. Astronaut. Aeronaut.* **135** 421–45
[14] Oran E S, Weber J E, Stefaniw E I, Lefebvre M H and Anderson J D 1998 A numerical study of two-dimensional H_2–O_2–Ar detonation using a detailed chemical reaction model *Combust. Flame* **113** 147–63
[15] Quirk J J 1993 Godunov-type schemes applied to detonation flows AD-A265482
[16] Sharpe G J 2001 Transverse waves in numerical simulations of cellular detonations *J. Fluid Mech.* **447** 31–51
[17] Shu C W and Osher S 1988 Efficient implementation of essentially non-oscillatory shock-capturing schemes *J. Comput. Phys* **77** 439–71
[18] Shu C W and Osher S 1989 Efficient implementation of essentially non-oscillatory shock-capturing schemes, II *J. Comput. Phys.* **83** 32–78
[19] Strehlow R A 1968 Gas phase detonations: recent developments *Combust. Flame* **12** 81–101
[20] Strehlow R A 1969 The nature of transverse waves in detonations *Astronaut. Acta* **14** 539–48
[21] Strehlow R A and Biller J R 1969 On the strength of transverse waves in gaseous detonations *Combust. Flame* **13** 577–82
[22] Strehlow R A and Crooker A J 1974 The structure of marginal detonations *Acta Astronaut.* **1** 303–15
[23] Stull D R 1971 *JANAF Thermochemical Tables, National Standard Reference Data Series* No. 37, 2nd edn (Gaithersburg, MD: US National Bureau of Standards)
[24] Subbotin V A 1975 Two kinds of transverse wave structure in multifront detonations *Combust. Explos. Shock Waves* **11** 83–8
[25] Taki S and Fujiwara T 1978 Numerical analysis of two-dimensional nonsteady detonations *AIAA J.* **16** 73–7
[26] Young T R 1979 CHEMEQ-Subroutine for solving stiff ordinary differential equations AD-A0835545
[27] Urtiew P A 1976 Idealized two-dimensional detonation waves in gaseous mixtures *Acta Astronaut.* **3** 187–200
[28] Voitsekhovskii B V, Mitrofanov V V and Topchian M E 1963 Structure of a detonation front in gases AD-633-821
[29] Wilson G J and MacCormack R W 1990 Modeling supersonic combustion using a fully-implicit numerical method AIAA-90-2307
[30] Zhang Z C, Yu S T and Hao H 2001 Direct calculations of two- and three-dimensional detonations by an extended CE/SE method AIAA-2001-0476